

A quantum mechanical analysis of the coherence de Broglie wavelength for superresolution and enhanced sensitivity in a coupled interferometer scheme

Byoung S. Ham^{1,2}

¹Department of Electrical Engineering and Computer Science, Gwangju Institute of Science and Technology, 123 Chumdangwagi-ro, Buk-gu, Gwangju 61005, South Korea

²Qu-Lidar, 123 Chumdangwagi-ro, Buk-gu, Gwangju 61005, South Korea

(February 20, 2026; bham@gist.ac.kr)

Abstract

Quantum sensing has drawn considerable attention as a means to overcome the fundamental limitations in classical sensing. In practice, however, quantum sensing has been strongly constrained by the photon loss, the achievable photon number N in $N00N$ states, and by a finite squeezing level in squeezed states. These limitations are particularly critical to photon-loss-sensitive applications such as LiDAR as well as to general sensing platforms that require large effective N , such as ring-laser gyroscopes. Recently, fundamentally different sensing platforms have been reported to overcome both classical and quantum constraints in a practical regime. One such approach exploits the coherence de Broglie wavelength (CBW) realized in an anti-symmetrically coupled Mach-Zehnder interferometer (MZI) architecture. Here, a pure quantum mechanical analysis of the CBW is presented for a loss-free sensing mechanism of superresolution with enhanced sensitivity. A proof-of-principle demonstration of CBW is also presented.

Introduction

Recently, a fundamentally different sensing metrology has been introduced and analyzed for the coherent superposition between classical light-based interferometers in the name of coherence de Broglie wavelength (CBW) [1,2]. Several proof-of-principle experiments of CBW using continuous waves [3] and single photons [4] have also been conducted for the demonstrations of not only photonic de Broglie wavelength (PBW)-like superresolution, but also unconditionally secured classical key distribution (USCKD) [5,6]. This new sensing technique of CBW is rooted in an antisymmetric coupling between identical Mach-Zehnder interferometers (MZIs) in a cascade scheme to satisfy $SU(2)$ group symmetry. Considering the MZI unitary transformation belonging to $SU(2)$, thus, CBW is for the N th power of the MZI unitary operator. To realize the N th power of a unitary transformation, the antisymmetric coupling between MZIs is essential to compensate for the input-output port exchange inherent to the coupled MZI geometry. As a result, N -times increased interference fringes are resulted in the output port of the CBW interferometer. Unlike N th-order intensity correlation in PBW quantum sensing [7-14], CBW is for the first-order intensity correlation compatible with classical sensing platforms [15-20]. Here, a pure quantum mechanical analysis of CBW is presented for an anti-symmetrically coupled MZI chain. The results are compared with PBW to understand its fundamental physics, uniqueness, distinction, and potential.

Precision measurements have drawn much attention over decades in both classical [15-20] and quantum sensing regimes [7-14,21-23]. In classical sensing platforms, the spatial resolution is generally governed by the diffraction limit. According to the Rayleigh criterion, the interferometric resolution is defined by the separation Δx between adjacent maxima and minima of interference fringes. To overcome the linear optics-based diffraction limit, nonlinear optics has been adapted to beat the diffraction limit in the order of magnitude enhanced spatial resolution [24,25]. Even in this case, the corresponding phase sensitivity still remains in the classical regime of the shot-noise limit (SNL) [26]. In a linear optics-based interferometric system, the diffraction limit has also been overcome via multi-wave interference using cavity or grating optics [15,27]. In these kinds of classical sensing platforms, the improvement factor is proportional to the number of superposed waves, resulting in several orders of magnitude enhancement in resolution. Although linear or nonlinear optics can improve phase resolution in a different degree of freedom, the major noise source in sensitivity is the electronic shot noise, far above the quantum limit. Thus, the classical sensing platform has recently been sought to reduce the electric noise close to the standard quantum limit or SNL using a single-photon detector array (SPDA) [28,29].

Quantum sensing relies on nonclassical light such as $N00N$ -based entangled photon pairs or squeezed states in a single-pass interferometric regime, such as an MZI [7-14]. The squeezed state has been successfully applied for a gravitational-wave measurement platform, such as LIGO [22], whose sensitivity gain is up to 15 dB [30].

On the other hand, the N00N-based quantum sensing has been studied to beat SNL using PBW [7-9], but has been challenged with the limited photon number N less than 20 [10]. In addition, lower-order harmonic contributions to the N th-order intensity correlation among N photons are intrinsically unavoidable [8,31]. Unlike squeezed light, the advantage of PBWs is superresolution with an effective wavelength $\lambda_{PBW} = \lambda_0/N$, where λ_0 is the wavelength of the input light. Because N00N states are generally achieved through spontaneous parametric down-conversion (SPDC) processes in nonlinear optics, their generation efficiency exponentially drops as N increases. A linear optics-based method faces a similar problem, where the highest order achieved so far is only $N = 18$, resulting in an impractical sensing platform [10]. Even with high N and high squeezing factor, quantum sensing is highly susceptible to photon loss, which restricts its applicability, particularly in remote-sensing applications such as LiDAR.

Results

Figure 1 shows a schematic of CBW in an anti-symmetrically coupled MZI chain [1,2]. The light source (L) in CBW may be either a conventional laser [3] or a single-photon source [4]. For laser illumination, the emitted photons are assumed to be independently and identically distributed (*i.i.d.*), satisfying the requirement of uncorrelated Fisher information [26]. CBW is compatible with coherence optics and thus interferometer-based optical sensors [15-17]. The consecutive coupling between opposite φ -MZIs via a dummy MZI ($\psi = 0$) is to accomplish the N -fold power of the MZI unitary operator U_{MZI} in a cascade structure. As a result, the N -coupled MZIs accumulate the unit phase φ by N times, resulting in N -accumulated phase $N\varphi$, satisfying CBW with $\lambda_{CBW}^{(N)} = \lambda_0/N$ [1-4]. Due to the satisfaction of SU(2) group symmetry, all lower-order harmonics are automatically eliminated in the output fields via the N th-order unitary transformation $(U_{MZI})^{\otimes N}$. Thus, CBW is fundamentally different from conventional wave optics, such as N slits, an N -grove grating, or an optical cavity, even though the observed resolution enhancement appears similar [27]. Unlike the N00N-based quantum sensing [12], whose measurement is for the N th-order intensity correlation among N -entangled photons, CBW is for the first-order intensity correlation of N coherent MZIs [1]. Unlike PBWs generating all orders of intensity products for a SPDC-generated N00N state [31], CBW generates only the N th-order product even for the same Hilbert space expansion 2^N [1,2]. Thus, CBW is inherent to a genuine order-filtering process in the coupled-MZI structure.

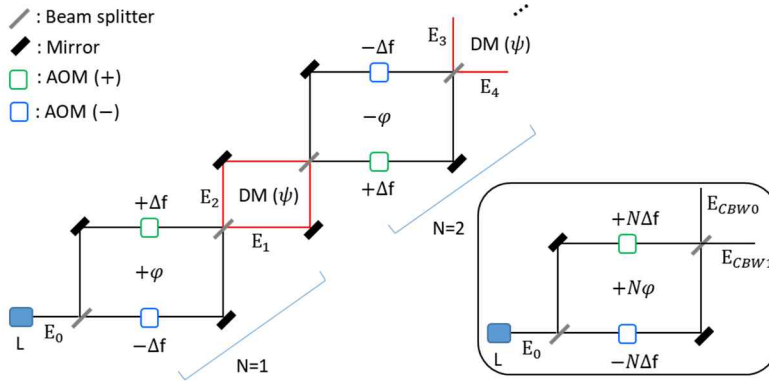


Fig. 1. Schematic of a coherence de Broglie wavelength. DM: dummy MZI, L: laser. Inset: effective MZI.

For the fully quantum mechanical analysis of CBW, we introduce logical bases of MZI corresponding to physical paths, $|0\rangle = |u\rangle$ and $|1\rangle = |l\rangle$, where u (l) indicates the upper (lower) path of MZI in Fig. 1. For an unknown phase φ , thus, each MZI can be treated as a two-level system, satisfying SU(2). For this, Pauli operators, σ_x and σ_z , are introduced to denote the photon population (bit flip) and rotation (phase) in a Bloch sphere model, where the bit flip is for output paths. Thus, the phase operator of MZI is set to be $Z(\varphi) = \begin{bmatrix} e^{i\varphi/2} & 0 \\ 0 & e^{-i\varphi/2} \end{bmatrix}$ for the first MZI in Fig. 1. Using the BS operator, $B = \frac{1}{\sqrt{2}} \begin{bmatrix} 1 & i \\ i & 1 \end{bmatrix}$, a single MZI unitary operator is induced: $U_{MZI}(\varphi) = BZB = e^{i\varphi} \sigma_x/2$. With a global phase $\varphi/2$ corresponding to the frequency detuning Δf in a no-loss MZI, the MZI unitary operator can be written as:

$$U_{MZI}(\varphi) = e^{i\varphi/2} \begin{bmatrix} \cos\left(\frac{\varphi}{2}\right) & \mathbf{\hat{m}} & \left(\frac{\varphi}{2}\right) \\ \mathbf{\hat{m}} & \left(\frac{\varphi}{2}\right) & \cos\left(\frac{\varphi}{2}\right) \end{bmatrix}. \quad (1)$$

Understanding Eq. (1) is for a unit MZI block in Fig. 1, the CBW unitary can be obtained by N -coupled MZIs in an antisymmetric coupling manner via a dummy MZI ($\psi = 2n\pi$):

$$U_{MZI}^{(N)}(\varphi) = (U_{MZI})^{\otimes N} = e^{N\varphi/2} \begin{bmatrix} \cos\left(\frac{N\varphi}{2}\right) & \mathbf{\hat{m}} & \left(\frac{N\varphi}{2}\right) \\ \mathbf{\hat{m}} & \left(\frac{N\varphi}{2}\right) & \cos\left(\frac{N\varphi}{2}\right) \end{bmatrix}. \quad (2)$$

Here, Eq. (2) cannot be obtained by a direct connection of identical MZIs without the dummy MZI due to $\sigma_z \sigma_z \neq \sigma_z$. Thus, the role of the dummy MZI (red) in Fig. 1 is critical for CBW to match the same logical bits:

$$D^\dagger \sigma_z D = \sigma_z, \quad (3)$$

where D denotes the dummy MZI operator, satisfying $[D, \sigma_z] = 0$. As coherently analyzed [1,2], thus, Eq. (2) results in CBW, mimicking PBW in the interference fringe pattern of superresolution. Unlike N -entangled photons interacting with the same MZI for PBW, CBW is for a single photon repeatedly interacting with N MZIs to coherently accumulate $N\varphi$, resulting in $U_{MZI}^{(N)}(\varphi)$. This phenomenon is the unique and distinctive feature of CBW. Using the Pauli operator, thus, Eq. (2) can also be rewritten as the unitary operator of CBW:

$$U_{CBW}^{(N)}(\varphi) = (e^{i\varphi\sigma_z/2})^N = e^{N\varphi\sigma_z/2}.$$

For a general input path-qubit state of MZI, $|\Psi_n\rangle = \alpha|0\rangle + \beta|1\rangle$, the output state of CBW can be represented as $|\Psi_N(\varphi)\rangle = U_{CBW}^{(N)}(\varphi)|\Psi_n\rangle$. In this format, the quantum state of CBW should be:

$$|\Psi_{CBW}\rangle = (|U\rangle + e^{N\varphi}|L\rangle)/\sqrt{2}, \quad (4)$$

where $|U\rangle$ and $|L\rangle$ stand for logical bases of CBW, satisfying $\sigma_z|U\rangle = +|U\rangle$ and $\sigma_z|L\rangle = -|L\rangle$. In comparison with PBW, $|\Psi_{PBW}\rangle = (|N, 0\rangle + e^{N\varphi}|0, N\rangle)/\sqrt{2}$, thus, $|\Psi_{CBW}\rangle$ represents N -coupled phase correlation in an effective MZI (see the Inset of Fig. 1). With a standard CBW input state, $|\Psi_n\rangle = |0\rangle$, the CBW output state is represented by $|\Psi_N(\varphi)\rangle = \omega\cos\left(\frac{N\varphi}{2}\right)|0\rangle + \mathbf{\hat{m}}\sin\left(\frac{N\varphi}{2}\right)|1\rangle$ (see Eq. (2)). As a result, the projection measurement probabilities of CBW in Fig. 1 are $P_1^{(N)} = \sin^2\left(\frac{N\varphi}{2}\right)$ and $P_0^{(N)} = \omega\cos^2\left(\frac{N\varphi}{2}\right)$. Thus, the same N -fold phase superresolution is obtained, as in PBW [7-14]. Here, the observable interference of both CBW and PBW is $P_0 \propto 1 + \omega\cos(N\varphi)$ and $P_1 \propto 1 - \omega\cos(N\varphi)$. The fundamental difference between CBW and PBW is in the origin of the effective wavelength reduction, where λ_{CBW} and λ_{PBW} arise from the operator power for the different natures of wave (phase) and particle (photon), respectively. In CBW, the order N is definitely and clearly determined by the number of MZIs in Fig. 1 due to the intrinsic MZI feature of $SU(2)$ group symmetry. In contrast, lower-order harmonics are inevitable in PBW because a particular $N00N$ state cannot be separated due to the intrinsic generation characteristics of the SPDC process [31,32], even if a coincidence detection method is used [31]. Lastly, there is no difference in $U_{CBW}^{(N)}(\varphi)$ between using a single photon and a continuous wave as the input light in Fig. 1 [3,4].

For Fisher information [26], the N -fold interference fringe of CBW can be represented as:

$$x_k = \mu(a + b\omega\cos(N\varphi + \varphi_0)) + n_k, \quad (5)$$

where $n_k \sim (0, \sigma^2)$, a is a DC offset, b is the visibility, and μ is the mean intensity of the detected signal. The n_k is individual noise given by the intensity noise variance σ^2 of the fixed input field. For M *i.i.d.* samples, the corresponding Fisher information $I(\varphi)$ is given by:

$$I(\varphi) = \frac{1}{\sigma^2} \sum_{k=0}^{M-1} \left(\frac{\partial x_k}{\partial \varphi}\right)^2. \quad (6)$$

With $\frac{\partial x_k}{\partial \varphi} = -b\mu N \mathbf{\hat{m}}\sin(N\varphi + \varphi_0)$, thus, $I_\varphi = \frac{b^2\mu^2 N^2}{\sigma^2} \sum_k \mathbf{\hat{m}}^2(N\varphi + \varphi_0)$ is obtained. For the optimal working point, the maximum Fisher information of CBW is $I_{max}(\varphi) = \frac{b^2\mu^2 N^2 M}{\sigma^2}$. As a result, the corresponding Cramer-Rao bound $\Delta\varphi_{CRLB} (\geq \frac{1}{\sqrt{I_\varphi}})$ is given by:

$$\Delta\varphi_{CRLB} \geq \frac{\sigma}{\mu|b|N\sqrt{M}}. \quad (7)$$

For a fixed input field μ , $\Delta\varphi \propto 1/N$ is obtained. Thus, the phase sensitivity of CBW in Fig. 1 seems to satisfy the Heisenberg limit with respect to the N φ -phase coupled MZIs [12]. By $I^{(M)}(\varphi) = NI^{(1)}(\varphi)$, CBW does not violate the *i.i.d.* assumptions, either, where the enhancement enters through the likelihood reparameterization $p(x|\varphi) = p(x|N\varphi)$ by the chain rule, $I_\varphi = N^2 I_\phi$. However, Fisher information is for the total resources involved according to the estimation theory [26]. For Eq. (7), the accountable MZI resource should scale N^2

for a fixed light μ . Thus, N^2 MZIs rather than N MZIs must be considered as *i.i.d.* random variables. In that sense, the resource N should be replaced by N^2 for fair comparison with M, resulting in $\Delta\varphi_{CRLB} \sim 1/\sqrt{N}$. CBW does not beat SNL. Unlike a single MZI, however, CBW gives N enhanced phase sensitivity for the random variables of μ of measured photons. From a practical point of view, CBW is also advantageous over N -limited PBW with high μ as well as high N .

For comparison purposes, the analytical solutions of the output fields in Fig. 1 have already been coherently derived for $N = 2$ [1,2]:

$$\begin{bmatrix} E_3 \\ E_4 \end{bmatrix} = [MZI]_2[\psi][MZI]_1 \begin{bmatrix} E_0 \\ 0 \end{bmatrix} = \frac{1}{2} \begin{bmatrix} -(1 - e^{i\psi})^2 - e^{i\psi}(1 + e^{i\psi})^2 & -i(1 - e^{2i\psi})(1 + e^{i\psi}) \\ i(1 - e^{2i\psi})(1 + e^{i\psi}) & -(1 + e^{i\psi})^2 - e^{i\psi}(1 - e^{i\psi})^2 \end{bmatrix} \begin{bmatrix} E_0 \\ 0 \end{bmatrix}. \quad (8)$$

For $\psi = 2n\pi$, $I_3 = \frac{I_0}{2}(1 + \cos 2\varphi)$ and $I_4 = \frac{I_0}{2}(1 - \cos 2\varphi)$ are obtained. This is the second-order ($N = 2$) CBW, resulting in doubled fringes in both output fields: $\lambda_{CBW}^{(2)} = \lambda_0/2$. For the extended CBW structure with coupled N MZIs of Fig. 1, generalized output fields are given by $I_{CBW0}^{(N)} = \frac{I_0}{2}(1 + \cos N\varphi)$ and $I_{CBW1}^{(N)} = \frac{I_0}{2}(1 - \cos N\varphi)$, as derived in Eq. (2) [1]. For $\psi = 2(n+1)\pi$, however, $I_3 = 0$ and $I_4 = I_0$ are obtained. This is the identity relation effective for USCKD, where the unconditional security is found in the randomness of MZI paths [5]. Thus, CBW and USCKD are considered as eigenmodes of the coupled MZIs.

Figure 2 shows numerical calculations of Eq. (8) as a function of φ and ψ . The left column is for $\psi = 0$, representing CBW in Eq. (2) [1,2]. The right column is for $\psi = \pi$, representing the identity relation applied for USCKD [5]. Considering the output intensity from a single MZI, e.g., I_1 and I_2 , whose phase modulation period is 2π or λ_0 , the period in the left column of Fig. 2 is doubled, representing $\lambda_{CBW}^{(2)} = \lambda_0/2$: This is the second-order CBW. By switching the dummy phase from $\psi = 0$ to $\psi = \pi$, the modulation fringes become frozen, resulting in an identity relation between the input (I_0) and outputs (I_4) (see the dashed lines in the top row). The same effect is also accomplished by controlling δf for a fixed ψ (see the Supplementary Materials or ref. 4).

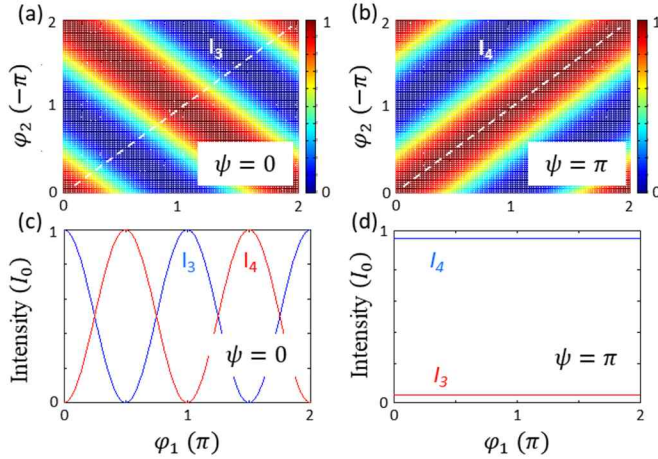


Fig. 2. Numerical calculations of Eq. (8). Intensities I_3 and I_4 as functions of φ_1 , φ_2 , and ψ . The dashed lines are for $\varphi_2 = -\varphi_1$. $I_j = E_j E_j^*$.

For the experimental demonstrations of CBW, the phase φ is replaced by a frequency control of $\pm\Delta f$ for CBW with $\psi = 0$ and for USCKD with $\psi = \pi$: $\pm\Delta\varphi = \pm\Delta f t$. The frequency offset Δf is controlled by the driving frequency of an acousto-optic modulator (AOM) pair in each MZI in Fig. 1. For this, both lower paths of MZIs are fixed at 80 MHz of AOMs. The upper path of AOM in the first (second) MZI is set at 80,000,001

(79,999,999) Hz, resulting in $\varphi = 2\pi t$. Thus, the modulation speed of the CBW moving frame in I_3 and I_4 is expected to be doubled at 2 Hz compared to a single MZI at 1 Hz, as shown in Fig. 2(c).

Figure 3 shows experimental demonstrations of CBW as well as USCKD for $N = 2$. Figure 3(a) shows CBW with a doubled modulation frequency at 2 Hz for $0 < t < 4$. At $t \sim 4$ s (see the left green arrow), one (E_1) of the dummy MZI paths is blocked, resulting in the demolition of the CBW with the modulation-frequency switching to 1 Hz (see the shaded area). By reopening the blocked dummy MZI path at $t \sim 8$ s (see the right green arrow), the 2 Hz modulation frequency of CBW is retrieved. Thus, the quantum mechanical analysis in Eqs. (2)-(4) is proven for CBW, where the origin of CBW is in the coherent superposition between consecutive MZIs via a dummy MZI, resulting in $(U_{MZI})^{\otimes N}$ for $N=2$. The observed CBW in the output intensity I_3 has the opposite pattern with respect to I_4 , as shown in Fig. 2(c) (see also the red and blue curves in Fig. 3(b)): For $N=3$ CBW, see ref. 4.

Figure 3(b) shows swapping between CBW [1] and USCKD [5], where the swapping occurs whenever the sign of Δf in the second MZI is reversed to be the same as the first MZI, or switching $\psi = 0$ to $\psi = \pi$ for a fixed Δf . USCKD results if the AOM driving frequency for the upper path ($-\Delta f$) of the second MZI is switched from 79,999,999 Hz to 80,000,000 Hz during $0 < t < 5$ in Fig. 3(b). The unwanted wiggles in the shaded area are mostly due to slightly misaligned MZI paths caused by AOM diffracted light. It can also be caused by air turbulence. As numerically calculated in Fig. 2(d), this identity relation between the input and output is due to a time-reversed double unitary transformation [5]. Because the sign reversal in Δf affects φ in the same way as ψ does [1], the dummy phase ψ can replace the Δf control function [6]. In other words, the same toggle switching between CBW and USCKD is obtained by an alternative basis choice of ψ , either 0 or π , for a fixed $\pm\Delta f$ configuration (see ref. 4).

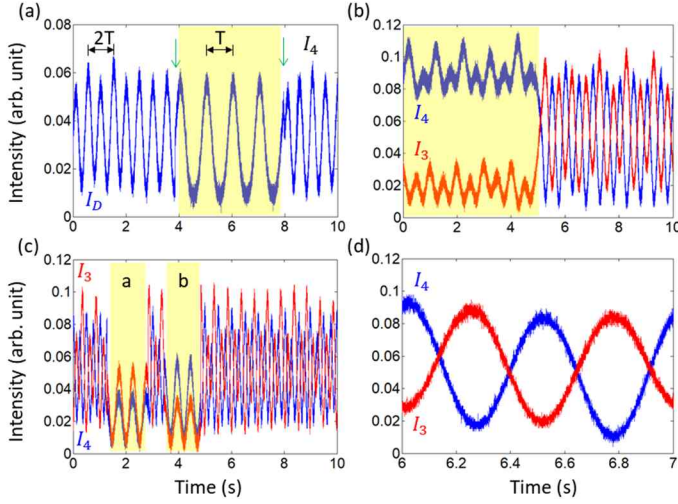


Fig. 3. Output intensities of Fig. 1 for CBW. (a) The CBW control with dummy MZI. The shaded area is with E_1 path blocking. The green arrows indicate switching time. T represents each modulation period of a single MZI. (b) CBW vs. USCKD with control of φ of the second MZI. The shaded areas are for USCKD by switching $-\varphi$ to $+\varphi$ of the second MZI. (c) CBW control with blocking one path of the φ -MZIs. (d) Expansion of (b).

In Fig. 3(c), details of CBW are experimentally conducted by blocking one of the control (φ) MZI paths, where the shaded a (b) is with the lower path blockage in the first (second) MZI in Fig. 1. The different intensities in the yellow-shaded areas are due to an unbalanced MZI caused by different efficiencies of AOMs. Thus, the observed doubling of the modulation frequency at 2 Hz provides a direct evidence of the unique feature of CBWs to surpass the diffraction limit. As coherently analyzed in Fig. 2 [1,2], the accumulated phase $N\varphi$ in the output fields increases linearly as the number (N) of coupled MZIs increases [4].

Figure 3(d) shows an extension of Fig. 3(b) for CBW, where the output intensities of I_3 and I_4 are out of

phase with each other. The calculated average CBW visibility is $V \sim 0.6$, where this non-perfect visibility is due to imperfect experimental conditions: For the near-perfect visibility of CBW, see ref. [4].

Conclusion

CBW was quantum mechanically analyzed to clarify the fundamental physics underlying PBW-like superresolution. The quantum nature of CBW was shown to originate from the N -powered unitary transformation of an MZI within anti-symmetrically coupled MZIs, which leads to N -fold accumulation of the unit phase. Furthermore, analysis based on Fisher information revealed N -enhanced phase sensitivity, even though CBW remains in the scope of SNL. Experimental demonstrations of CBW were conducted and analyzed to validate the theoretical predictions. These results established that CBW operates on fundamentally different principles from classical sensing mechanisms, achieving superresolution and enhanced sensitivity that are unattainable in classical physics. Understanding the practical limitations of quantum sensing, such as photon loss, finite N , and the presence of unavoidable lower-order intensity components, CBW shows strong potential for remote sensing applications. In particular, CBW offers the prospect of N -scalable superresolution with near-perfect visibility and \sqrt{N} -enhanced sensitivity.

Methods

In Fig. 1, acousto-optic modulators (AOMs) are employed to realize frequency-dependent phase control. Phase tuning in the MZI is achieved via AOM-induced frequency offsets, $\pm\delta f$, which are generated by synchronized RF sources (PTS160, PTS250, and two-channel Tektronix AFG3102). As a result, the original path-length-dependent CBW scheme [1] is replaced by an AOM-based CBW implementation controlled by RF driving frequencies. The coherent input field E_0 is generated by a Toptica AT-SHG pro laser at a wavelength of 605.966 nm with a linewidth of approximately 300 kHz. Thus, the 1 Hz frequency offset introduced between the two arms of the MZI in Fig. 1 is to generate interference fringes in the time domain, while remaining well within the MZI coherence. Under typical laboratory conditions without passive or active stabilization controls, the MZI remains stable for several minutes. To maintain adequate AOM diffraction efficiency in the second MZI, the beam diameter is reduced using a pair of convex lenses positioned around each AOM. The CBW performance is insensitive to the input laser power, which is maintained at a few mW throughout the experiment. For the measurements shown in Fig. 3, Hamamatsu avalanche photodiodes (C12703) are used in conjunction with a Tektronix oscilloscope (DPO5204B). An iris is inserted to isolate the zeroth-order fringe and use the first-order diffracted lights for CBW. For the Supplementary movies, the output intensities I_C and I_D are projected onto a paper screen and recorded using iPhones. The frequency offset $\pm\delta f$ between two upper MZI arms is controlled by a two-channel arbitrary function generator (Tektronix AFG3102) with a frequency resolution of 0.001 Hz. All data in Figs. 3 are raw single-shot measurements without averaging or postprocessing. Each MZI arm has a path-length of approximately 60 cm. Overall, the experimental setup is intentionally simple and unshielded, operating in a coarse and noisy laboratory environment.

Data availability

All data generated or analyzed during this study are included in the published article.

References

1. Ham, B. S. Deterministic control of photonic de Broglie waves using coherence optics. *Sci. Rep.* **10**, 12899 (2020).
2. Hamm B. S. Analysis of nonclassical features in a coupled macroscopic binary system. *New J. Phys.* **22**, 123043 (2020).
3. Ham, B. S. Observations of coherence de Broglie waves. arXiv:2007.04738 (2020).
4. Kim, S. & Ham, B. S. Experimental demonstrations of coherence de Broglie waves using sub-Poisson distributed coherent photon pairs. arXiv:2107.10136 (2021).
5. Ham, B. S. Unconditionally secured classical cryptography using quantum superposition and unitary transformation. *Sci. Rep.* **10**, 11687 (2020)
6. Ham, B. S. Experimental demonstrations of unconditional security in a purely classical regime. *Sci. Rep.* **11**, 4149 (2021).

7. Jacobson, J., Gjörk, G., Chung, I. & Yamamoto, Y. Photonic de Broglie waves. *Phys. Rev. Lett.* **74**, 4835-4838 (1995).
8. Edamatsu, K., Shimizu, R. & Itoh, T. Measurement of the photonic de Broglie wavelength of entangled photon pairs generated by parametric down-conversion. *Phys. Rev. Lett.* **89**, 213601 (2002).
9. Walther, P., Pan, J.-W., Aspelmeyer, M., Ursin, R., Gasparon, S. & Zeilinger, A. De Broglie wavelength of a non-local four-photon state. *Nature* **429**, 158-161 (2004).
10. Wang, X.-L. et al., 18-qubit entanglement with six photons' three degree of freedom. *Phys. Rev. Lett.* **120**, 260502 (2018).
11. Dowling, J. P. Quantum optical technologies for metrology, sensing, and imaging. *J. Lightwave Tech.* **33**, 2359-2370 (2015).
12. Giovannetti, V., Lloyd, S. & Maccone, L. Quantum-enhanced measurements: beating the standard quantum limit. *Science* **306**, 1330-1336 (2004).
13. Leibfried, D. et al. Toward Heisenberg-limited spectroscopy with multiparticle entangled states. *Science* **304**, 1476-1478 (2004).
14. Dowling, J.P. Quantum optical metrology—The lowdown on high-N00N states. *Contemp. Phys.* **49**, 125–143 (2008).
15. Hariharan, P. Optical interferometry, 2nd Ed. (Academic Press, New York, 2003).
16. McGrew, W. F. et al. Atomic clock performance enabling geodesy below the centimeter level. *Nature* **564**, 87-90 (2018).
17. Jonkman, J., Brown, C. M., Wright, G. D., Anderson, K. I. & North, A. J. Tutorial: guidance for quantitative confocal microscopy. *Nature Protocols* **15**, 1585-1611 (2020).
18. Isbell, J. W. et al. Direct imaging of active galactic nucleus outflows and their origin with the 23 m large binocular telescope. *Nature Astro.* **9**, 417-427 (2025).
19. Luetzenburg, G., Kroon, A., Kjeldsen, K. K., Splinter, K. D. & Bjork, A. A. High-resolution topographic surveying and change detection with the iPhone LiDAR. *Nature Protocols* **19**, 3520-3541 (2024).
20. Vicidomini, G.; Bianchini, P.; Diaspro, A. STED super-resolved microscopy. *Nature Methods*, **15**, 173-182 (2018)
21. Degen, C. L., Reinhard, F. & Cappellaro, P. Quantum sensing. *Rev. Mod. Phys.* **89**, 035002 (2017).
22. Tse, M. et al. Quantum-enhanced advanced LIGO detectors in the era of gravitational-wave astronomy. *Phys. Rev. Lett.* **123**, 231107 (2019).
23. Boto, A. N. et al. Quantum interferometric optical lithography: exploiting entanglement to beat the diffraction limit. *Phys. Rev. Lett.* **85**, 2733-2736 (2000).
24. Hell, S. W. Nanoscopy with focused light (Nobel lecture). *Angew. Chem. Int. Ed.* **54**, 8054-8066 (2015).
25. Fujimoto, J. G., Pitris, C., Boppart, S. A. and Brezinski, M. E. Optical coherence tomography: an emerging technology for biomedical imaging and optical biopsy. *Neoplasia* **2**, 9-25 (2000).
26. Kay, S. *Fundamentals of statistical signal processing: Estimation theory* (Prentice Hall, New Jersey 1993).
27. Pedrotti, F.L., Pedrotti, L.M., Pedrotti, L.S. *Introduction to Optics*, 3rd ed. (Pearson Education, Inc.: London, UK, 2007).
28. Charbon, E., Fisshburn, M., Walker, R., Henderson, R. K. & Niclass, C. *SPAD-based sensors*, Eds. F. Remondino and D. Stoppa (Springer-Verlag, Berlin, 2013).
29. Scholes, S., Mora-Martin, G., Zhu, F., Gyongy, I., Soan, P. & Leach, J. Fundamental limits to depth imaging with single-photon detector array sensors.” *Sci. Rep.* **13**, 176 (2023).
30. Vahlbruch, H. et al. Detection of 15 dB squeezed states of light and their application for the absolute calibration of photoelectric quantum efficiency. *Phys. Rev. Lett.* **117**, 110801 (2016).
31. Sun, F. W. et al. Experimental demonstration of phase measurement precision beating standard quantum limit by projection measurement. *EPL* **82**, 24001 (2008).
32. Nagata, T., Okamoto, R., O’Brian, J. L., Sasaki, K. & Takeuchi, S. “Beating the standard quantum limit with four-entangled photons,” *Science* **316**, 726–729 (2007).

Author contribution

B.S.H. conceived the idea and solely wrote the paper.

Funding

The author acknowledges that this work was supported by the IITP-ITRC grant (IITP 2026-RS-2021-II211810) funded by the Korean government (Ministry of Science and ICT).

Competing interests

The author is the founder of Qu-Lidar.

Additional information

Supplementary Information The online version contains supplementary material available at